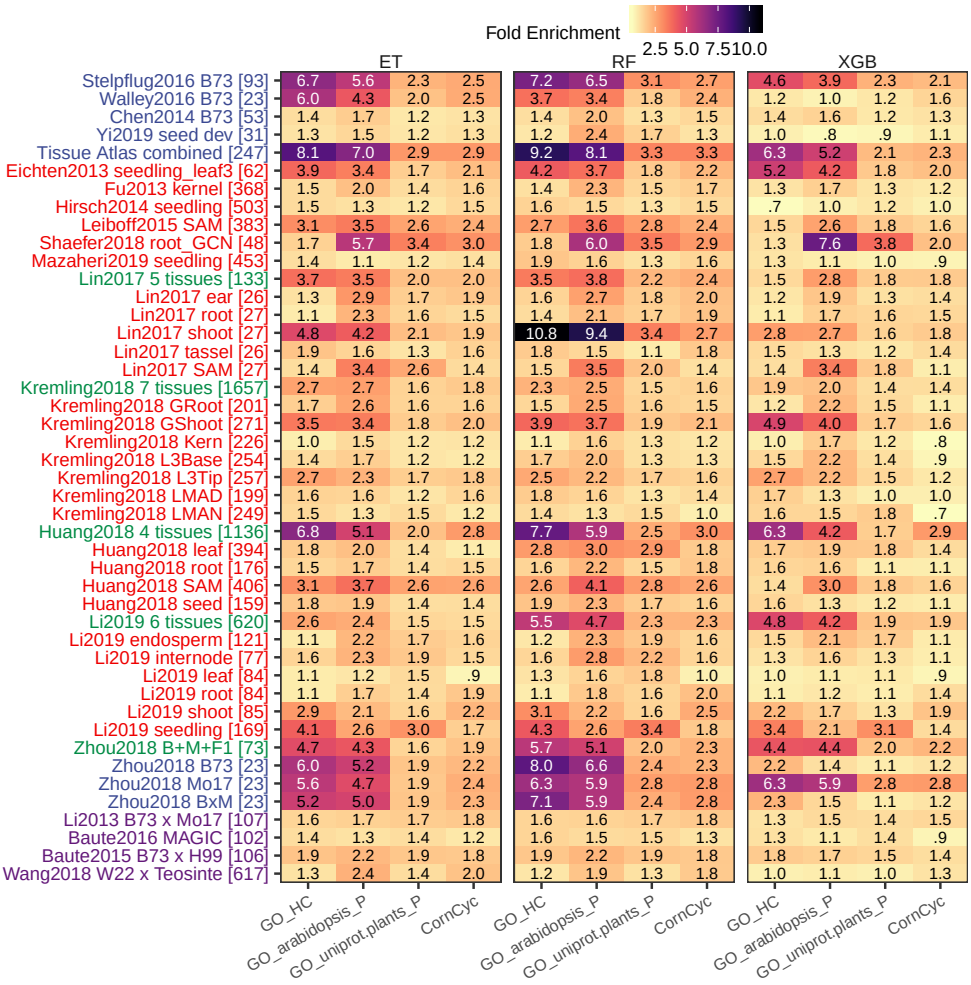

Figure S1. Comparison of GRNs built with different methods according to enrichment of functional annotations (Gene Ontology, CornCyc, etc). For each network only the top 100,000 predicted TF-target associations were taken. Fold enrichment is calculated as the observed number of shared GO/CornCyc terms (by targets regulated by a common TF) divided by the expected number of shared annotation terms (determined by permutation). The names for each of the networks are color-coded to indicate B73 developmental surveys (blue), genotype surveys (red), meta-networks (green) or previously generated GRNs (teal). Each GRN was built using three regression methods: RF (random forest), ET (extra trees) and XGB (gradient boosting). These analyses were used to select the approach used to generate analyses for Figure 1.

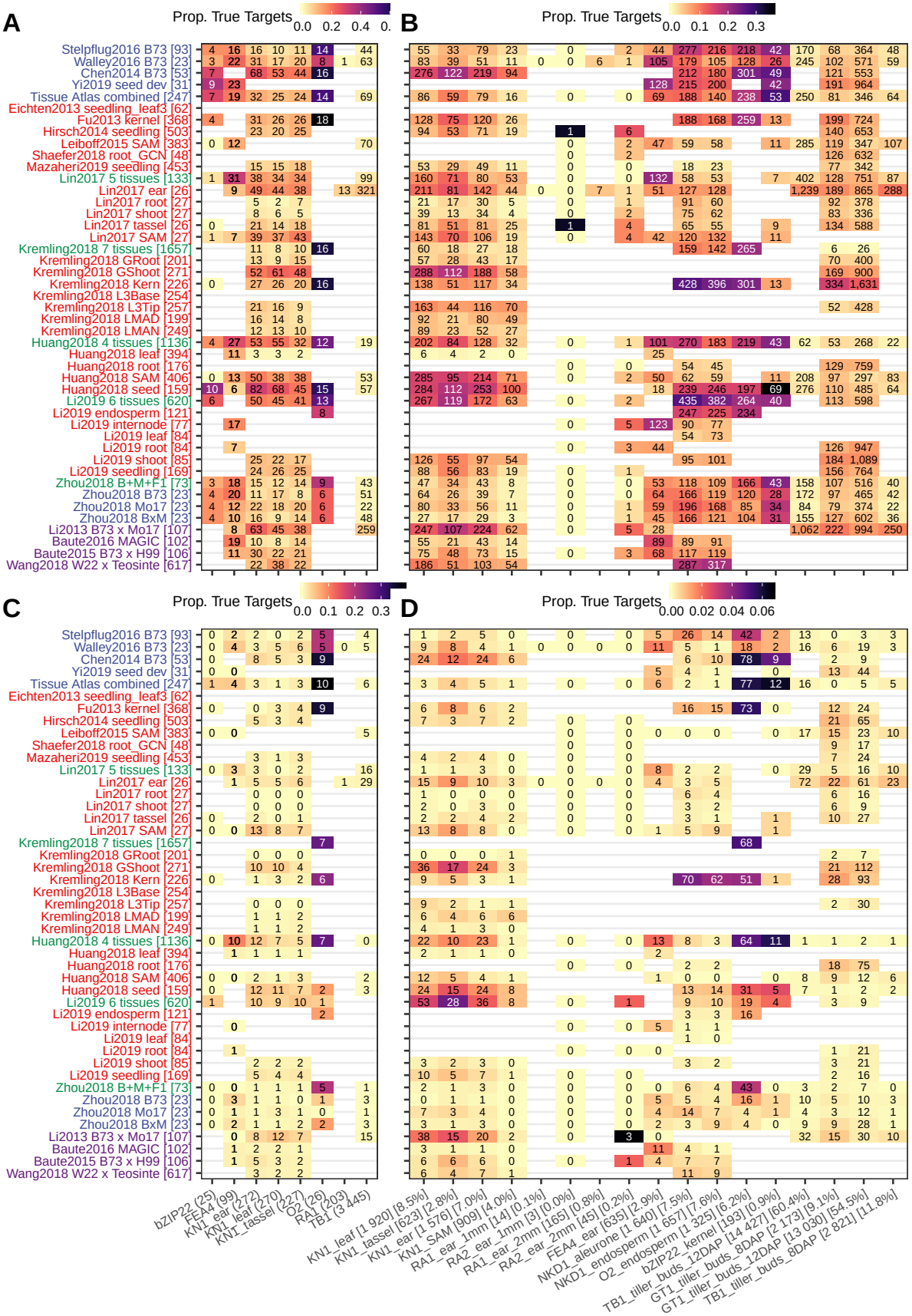
A
Prop. True Targets
0.0 0.2 0.4 0.
B
Prop. True Targets
0.0 0.1 0.2 0.3
C
Prop. True Targets
0.0 0.1 0.2 0.3
D
Prop. True Targets
0.00 0.02 0.04 0.06
Stelpflug2016 B73 [93]
Walley2016 B73 [23]
Chen2014 B73 [53]
Yi2019 seed dev [31]
Tissue Atlas combined [247]
Eichten2013 seedling_leaf3 [62]
Fu2013 kernel [368]
Hirsch2014 seedling [503]
Leiboff2015 SAM [383]
Shaefer2018 root_GCN [48]
Mazaheri2019 seedling [453]
Lin2017 5 tissues [133]
Lin2017 ear [26]
Lin2017 root [27]
Lin2017 shoot [27]
Lin2017 tassel [26]
Lin2017 SAM [27]
Kremling2018 7 tissues [1657]
Kremling2018 GRoot [201]
Kremling2018 GShoot [271]
Kremling2018 Kern [226]
Kremling2018 L3Base [254]
Kremling2018 L3Tip [257]
Kremling2018 LMAD [199]
Kremling2018 LMAN [249]
Huang2018 4 tissues [1136]
Huang2018 leaf [394]
Huang2018 root [176]
Huang2018 SAM [406]
Huang2018 seed [159]
Li2019 6 tissues [620]
Li2019 endosperm [121]
Li2019 internode [77]
Li2019 leaf [84]
Li2019 root [84]
Li2019 shoot [85]
Li2019 seedling [169]
Zhou2018 B+M+F1 [73]
Zhou2018 B73 [23]
Zhou2018 Mo17 [23]
Zhou2018 BxM [23]
Li2013 B73 x Mo17 [107]
Baute2016 MAGIC [102]
Baute2015 B73 x H99 [106]
Wang2018 W22 x Teosinte [617]
bZIP22 (25)
FEA4 (99)
KN1_ear (272)
KN1_leaf (270)
KN1_tassel (227)
O2 (26)
RA1 (203)
TB1 (3 445)
KN1_leaf [1 920] [8.5%]
KN1_tassel [623] [2.8%]
KN1_ear [1 576] [7.0%]
KN1_SAM [909] [4.0%]
RA1_ear_1mm [14] [0.1%]
RA2_ear_1mm [3] [0.0%]
RA2_ear_2mm [165] [0.8%]
RA1_ear_2mm [45] [0.2%]
FEA4_ear [635] [2.9%]
NKD1_aleurone [1 640] [7.5%]
NKD1_endosperm [1 657] [7.6%]
O2_endosperm [1 325] [6.2%]
bZIP22_kernel [193] [0.9%]
TB1_tiller_buds_12DAP [14 427] [60.4%]
GT1_tiller_buds_8DAP [2 173] [9.1%]
GT1_tiller_buds_12DAP [13 030] [54.5%]
TB1_tiller_buds_8DAP [2 821] [11.8%]

Figure S2. Number of true TF targets captured by the top 1 million predictions (A-B) and the top 100k predictions (C-D) in each GRN. (A) and (C): direct targets of published TF studies derived from ChIP-Seq and mutant RNA-Seq experiments; (B) and (D) For each one of the 17 maize TFs with knockout mutant RNA-Seq data available, differentially expressed genes between mutant and wildtype were identified using DESeq2 (p-value < 0.01). Numbers in each cell represent the actual number of true targets captured by each GRN during each evaluation, while cells were colored based on the proportion of captured true targets. Blank (white) cells stand for missing data where the TF being evaluated is not expressed or not variable (i.e., zero variance) in the corresponding GRN. Y-axis labels correspond to the different networks listed in Table 1. X-axis labels (e.g., "KN1_ear (272)" or "KN1_ear [1576] [7.0%]") represent the common name for each TF, the tissue in which the TF is expressed, followed by the number of direct targets (Panels A and C) or number and proportion of differentially expressed genes in TF mutant (Panels B and D). The information in this figure supports the choice of analyses parameters used for Figure 1 and 2.

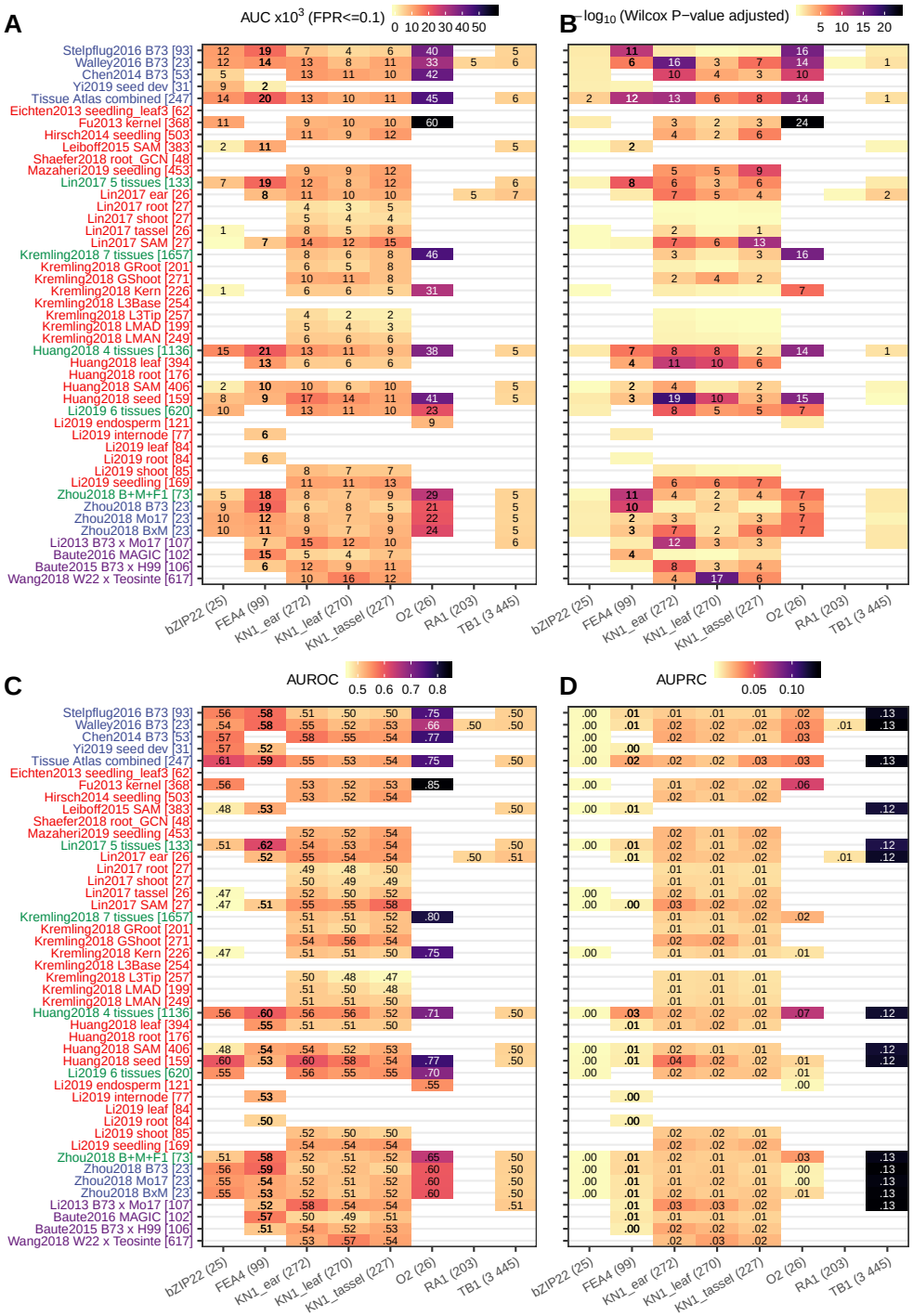

Figure S3. Evaluation of GRNs using support from direct targets of 8 known TFs. (A) Area under receiver-operating characteristic curve (AUROC) until an False Positive Rate of 0.1 is reached; (B) Wilcox rank test performed using the predicted (TF-target) interaction scores between the group of true targets (DEGs) and non-targets (non-DEGs); (C) Area under receiver-operating characteristic curve (AUROC) and (D) Area under precision-recall curve (AUPRC). Light yellow cells with no numbers stand for "not significant" ($P > 0.05$), while blank (white) cells stand for missing data where the TF being evaluated is not expressed or not variable (i.e., zero variance) in the corresponding GRN. This analysis provides further support for the analyses in Figure 1A.

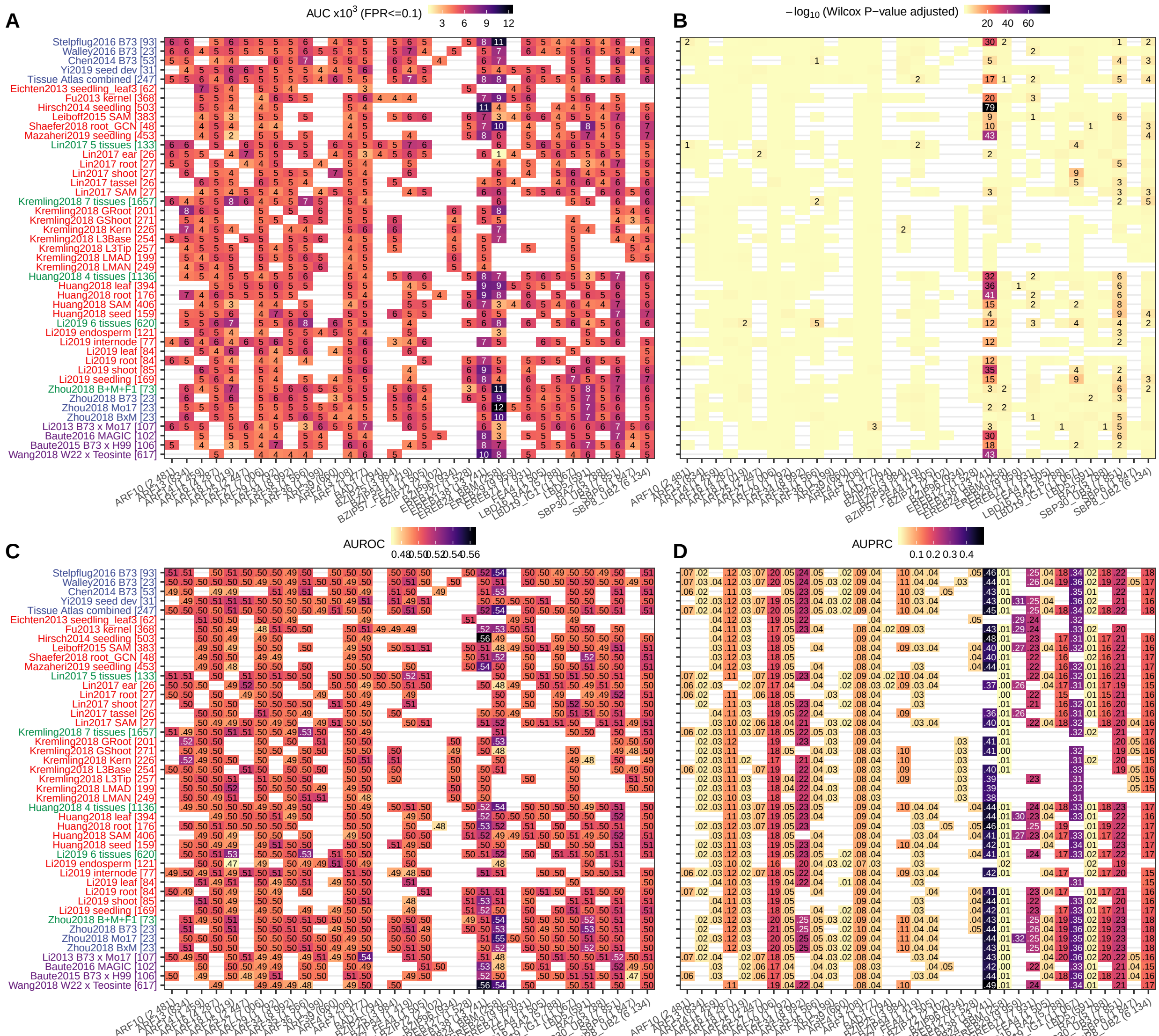

Figure S4. Evaluation of GRNs using support from 31 maize TF DAP-Seq datasets. (A) Area under receiver-operating characteristic curve (AUROC) until an False Positive Rate of 0.1 is reached; (B) Wilcox rank test performed using the predicted (TF-target) interaction scores between the group of true targets (DEGs) and non-targets (non-DEGs); (C) Area under receiver-operating characteristic curve (AUROC) and (D) Area under precision-recall curve (AUPRC). Light yellow cells with no numbers stand for "not significant" (P > 0.05), while blank (white) cells stand for missing data where the TF being evaluated is not expressed or not variable (i.e., zero variance) in the corresponding GRN. These analyses provide further support for the findings in Figure 1.

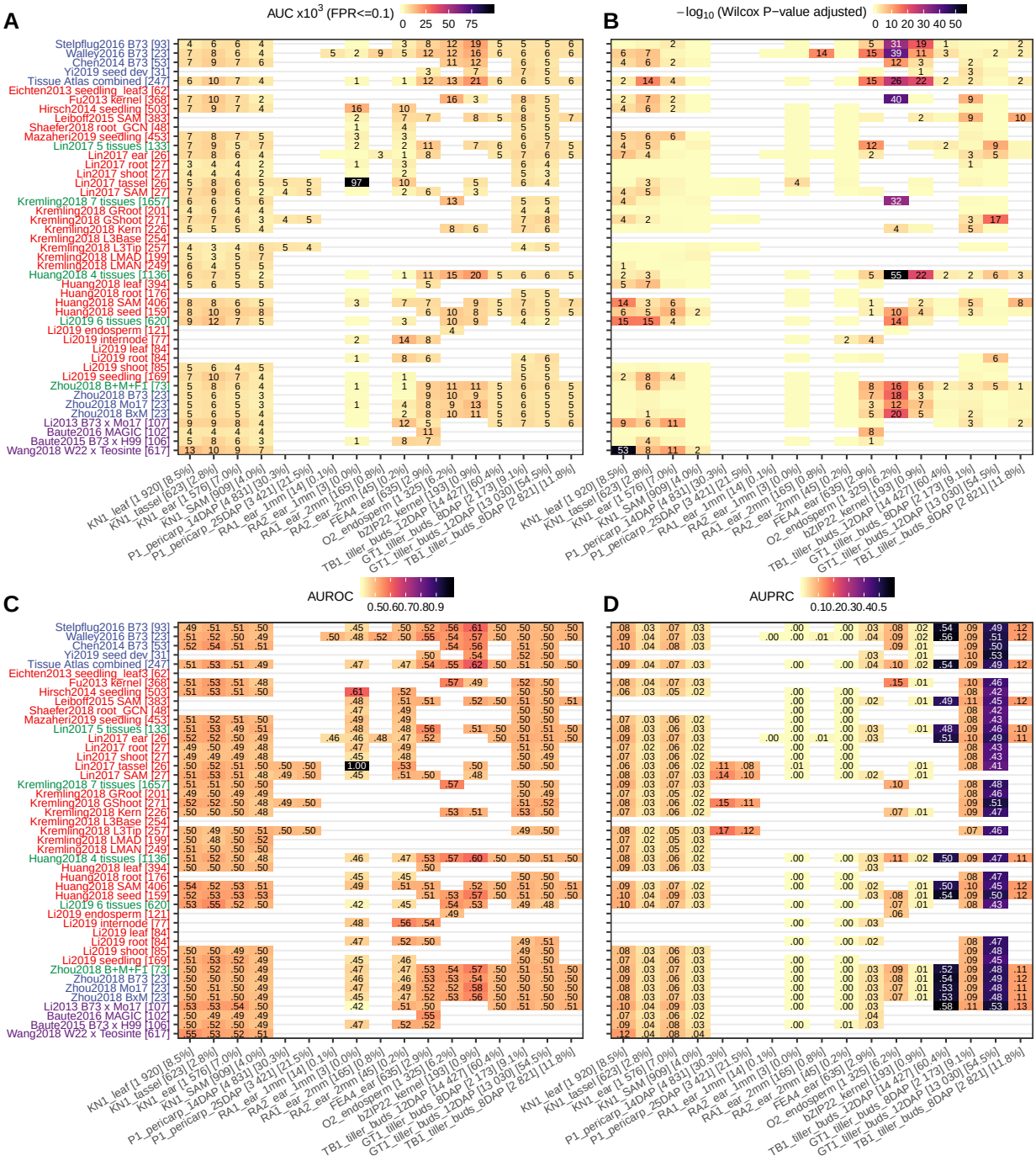

Figure S5. Evaluation of GRNs using support from 17 maize TF knockout mutants RNA-Seq datasets. (A) Area under receiver-operating characteristic curve (AUROC) until an False Positive Rate of 0.1 is reached; (B) Wilcox rank test performed using the predicted (TF-target) interaction scores between the group of true targets (DEGs) and non-targets (non-DEGs); (C) Area under receiver-operating characteristic curve (AUROC) and (D) Area under precision-recall curve (AUPRC). Light yellow cells with no numbers stand for "not significant" ($P > 0.05$), while blank (white) cells stand for missing data where the TF being evaluated is not expressed or not variable (i.e., zero variance) in the corresponding GRN. These analyses provide further support for the findings in Figure 1.

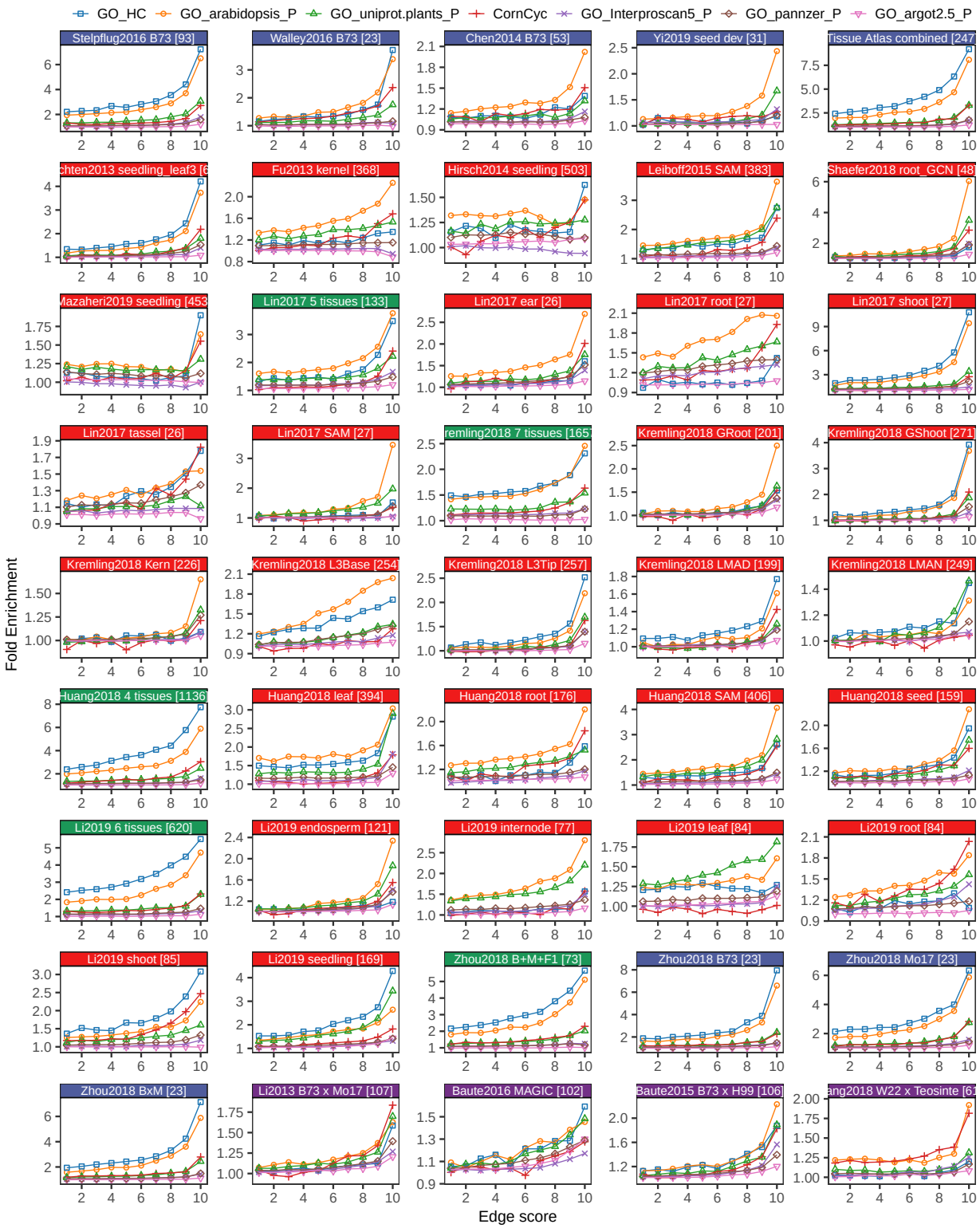

Figure S6. Enrichment of co-annotated GO/CornCyc terms in co-regulated network targets. For each network the top 1 million predicted TF-target associations were binned to 10 bins and assessed for enrichment of GO/CornCyc functional annotation. Fold enrichment is calculated as the observed number of shared GO/CornCyc terms (by targets regulated by a common TF) divided by the expected number of

shared annotation terms (determined by permutation). The names for each of the networks are color coded to indicate B73 developmental surveys (blue), genotype surveys (red), meta-networks (green) or previously generated GRNs (teal). A total of six sources of GO annotation were used: GO_HC (high quality hand-curated terms transferred from maize AGP_v3 annotation), GO_arabidopsis, GO_uniprot.plants, GO_Interproscan5, GO_pannzer and GO_argot2.5. These visualizations are the same as what is presented in Figure 2A but show the patterns for all co-expression networks.

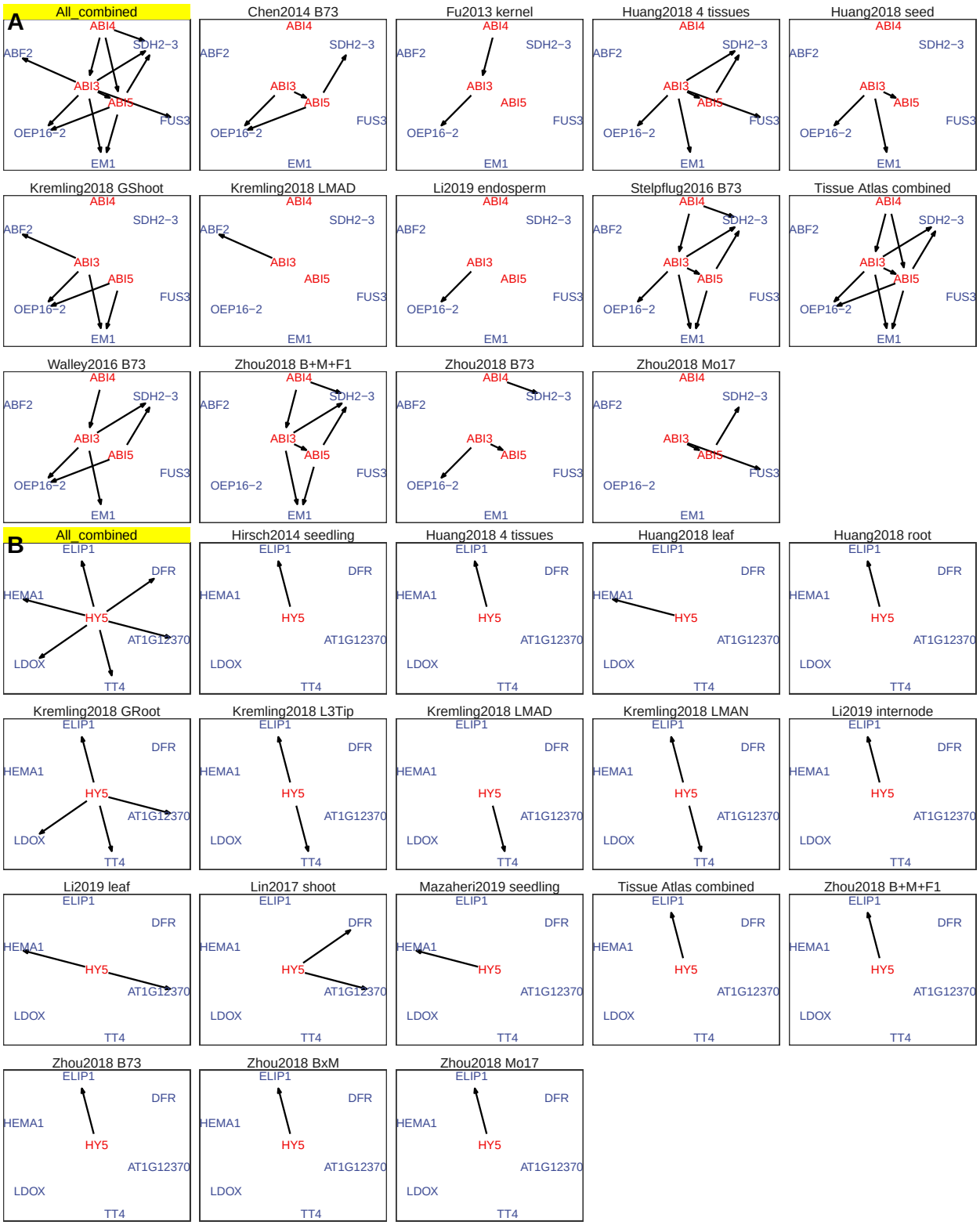

Figure S7. Different GRNs capture distinct parts of documented transcriptional regulations from Arabidopsis for the abscisic acid (ABA) pathway (A) and HY5 (Elongated Hypocotyl 5) regulated pathway (B). These visualizations provide a detailed view of the data currently presented in Figure 3B and 3C.

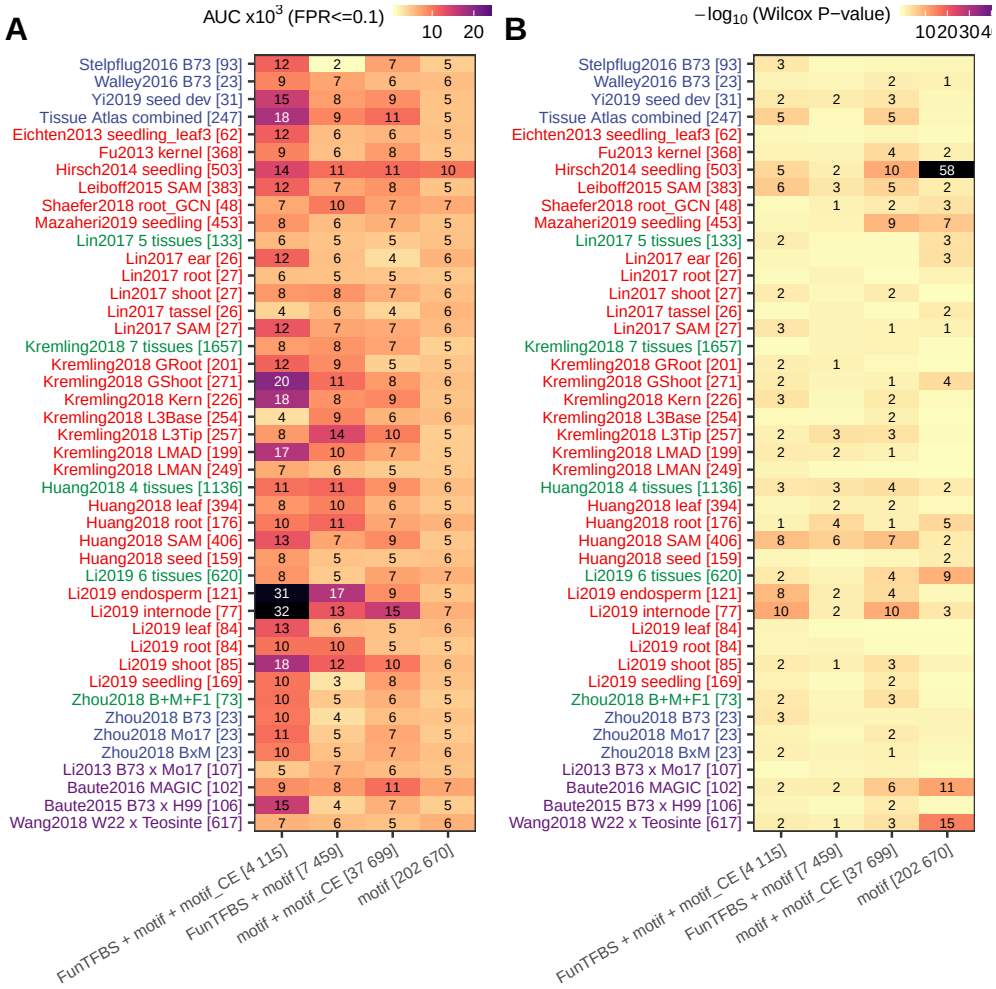

Figure S8. Evaluation (AUROC and Wilcox P-value) of constructed GRNs using four sets of predicted TF-target interactions based on TF-binding site motif, conserved element of TFBS motif or FunTFBS. There are 202,670 “motif”-based predictions, 37,699 predictions based on motif and cross-species conservation, 7,459 predictions based on motif and FunTFBS as well as 4,115 predictions based on all three evidences. This figure provides the specific values for interpretations that are made in the results section.

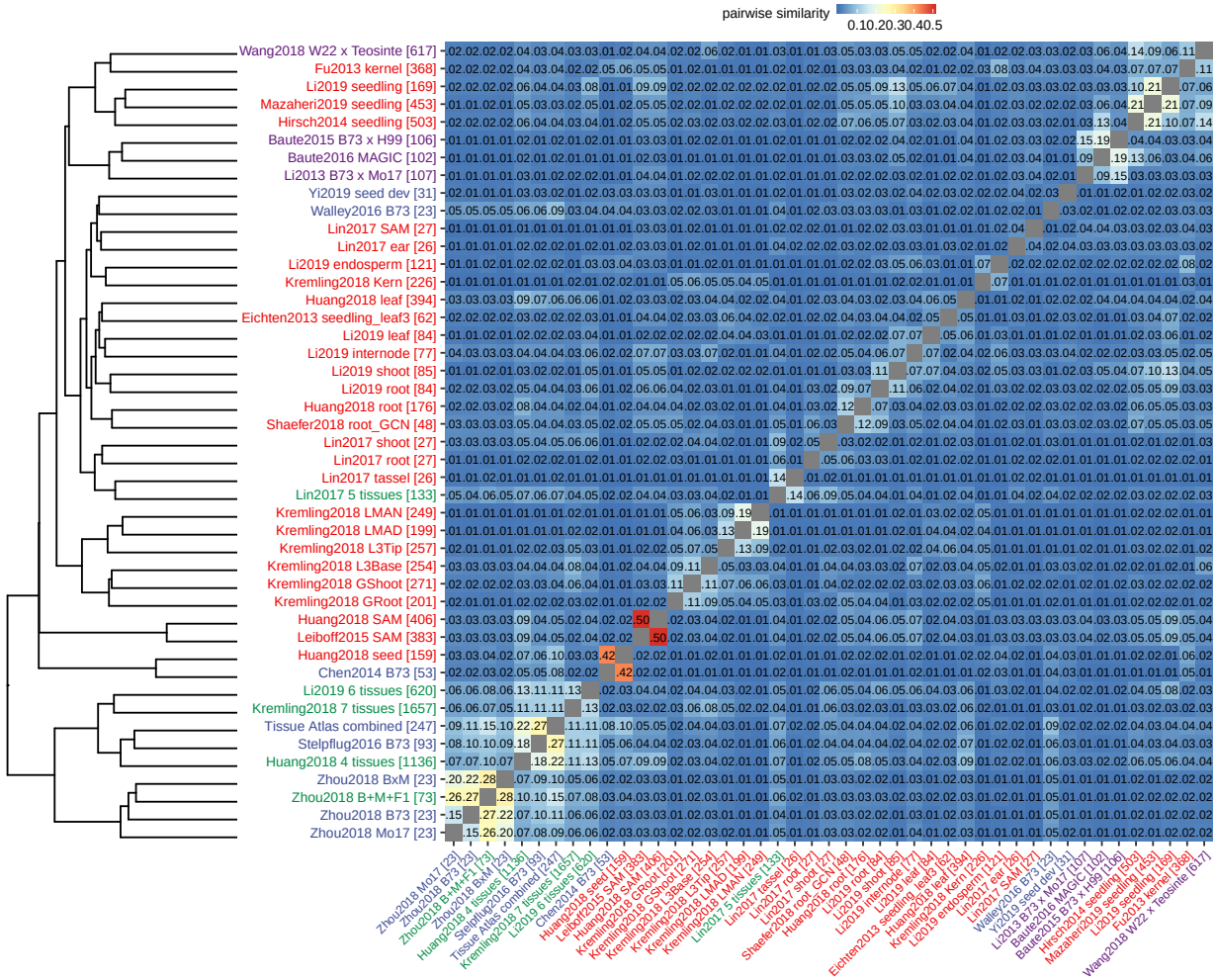

Figure S9. Hierarchical clustering of 45 GRNs. Pairwise distance between networks was determined by taking the top 100,000 TF-target predictions from each network and calculating the proportion of shared (common) predictions (using 'dist()' function in R with additional argument 'method=binary'). Hierarchical clustering was then performed based on the cross-network pairwise distance matrix using "ward.D" method. This supporting figure provides a visualization to support the interpretations of Figure 3 and 4.

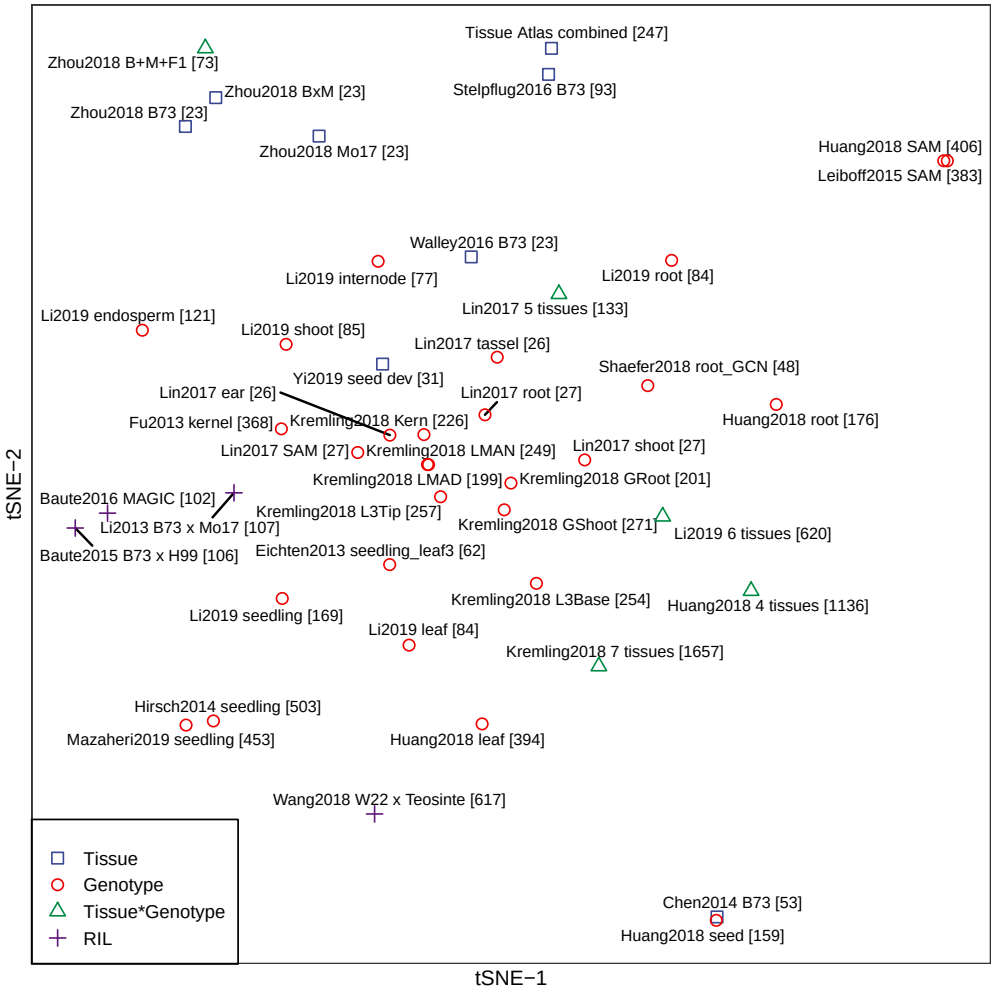

Figure S10. T-SNE clustering of 45 GRNs. Top 500,000 TF-target predictions were extracted from each network to perform t-SNE clustering using parameter “perplexing=9, permutation=2000”. This supporting figure provides a visualization to support the interpretations of Figure 3 and 4.

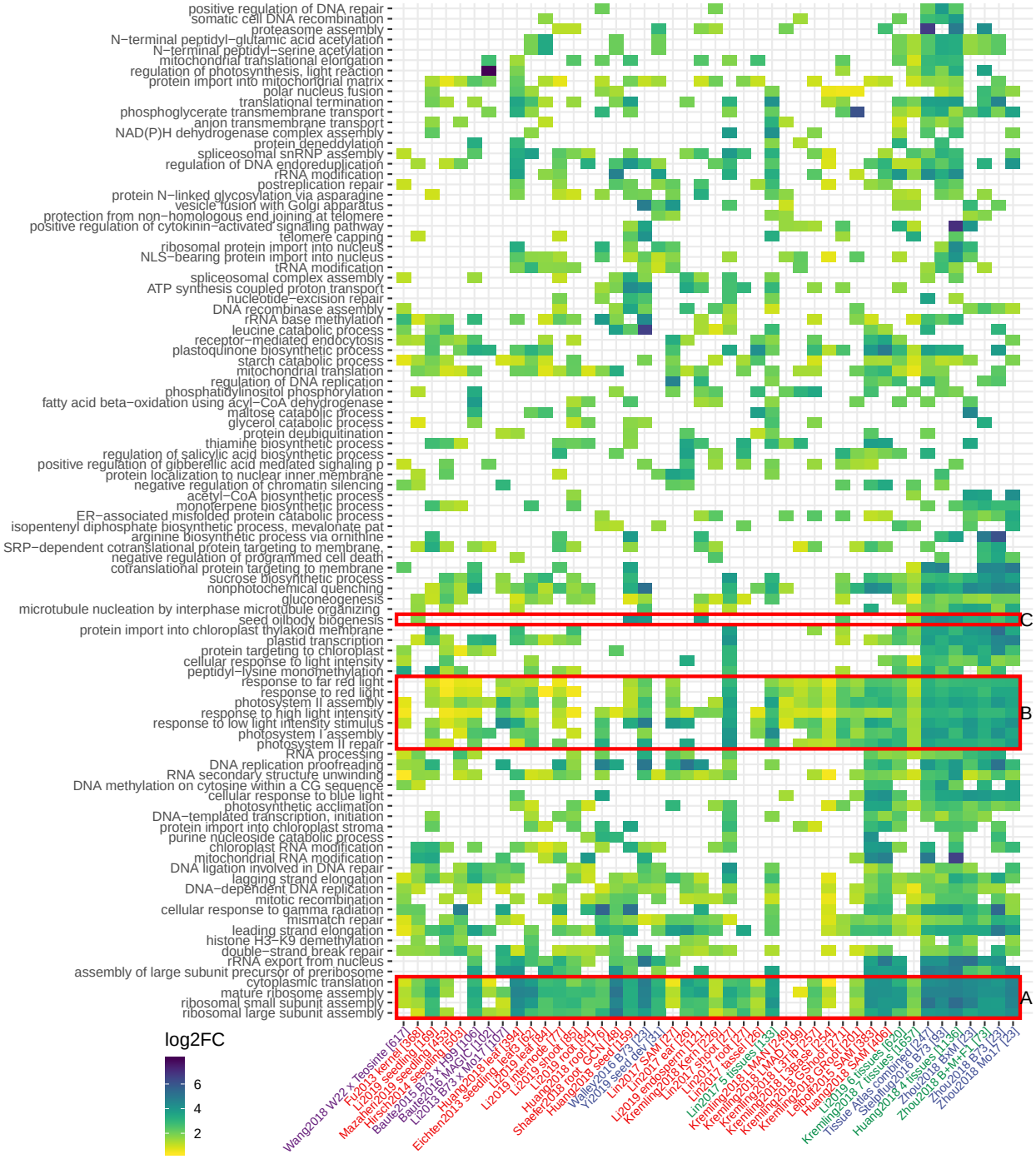

Figure S11. Hierarchical clustering of 98 Gene Ontology (Uniprot.Plants, level 6) terms using fold enrichment in different GRNs. Only GO terms enriched (i.e., P-value < 0.05 and fold change > 1, top 100k edges taken) in at least 3 out of the 44 networks were used for clustering. Insignificant enrichment (p-value < 0.05) was treated as missing data and shown as white space in the figure. Fold enrichment is determined as described in Figure 2. This supporting figure provides a visualization to support the interpretations of Figure 2-4.

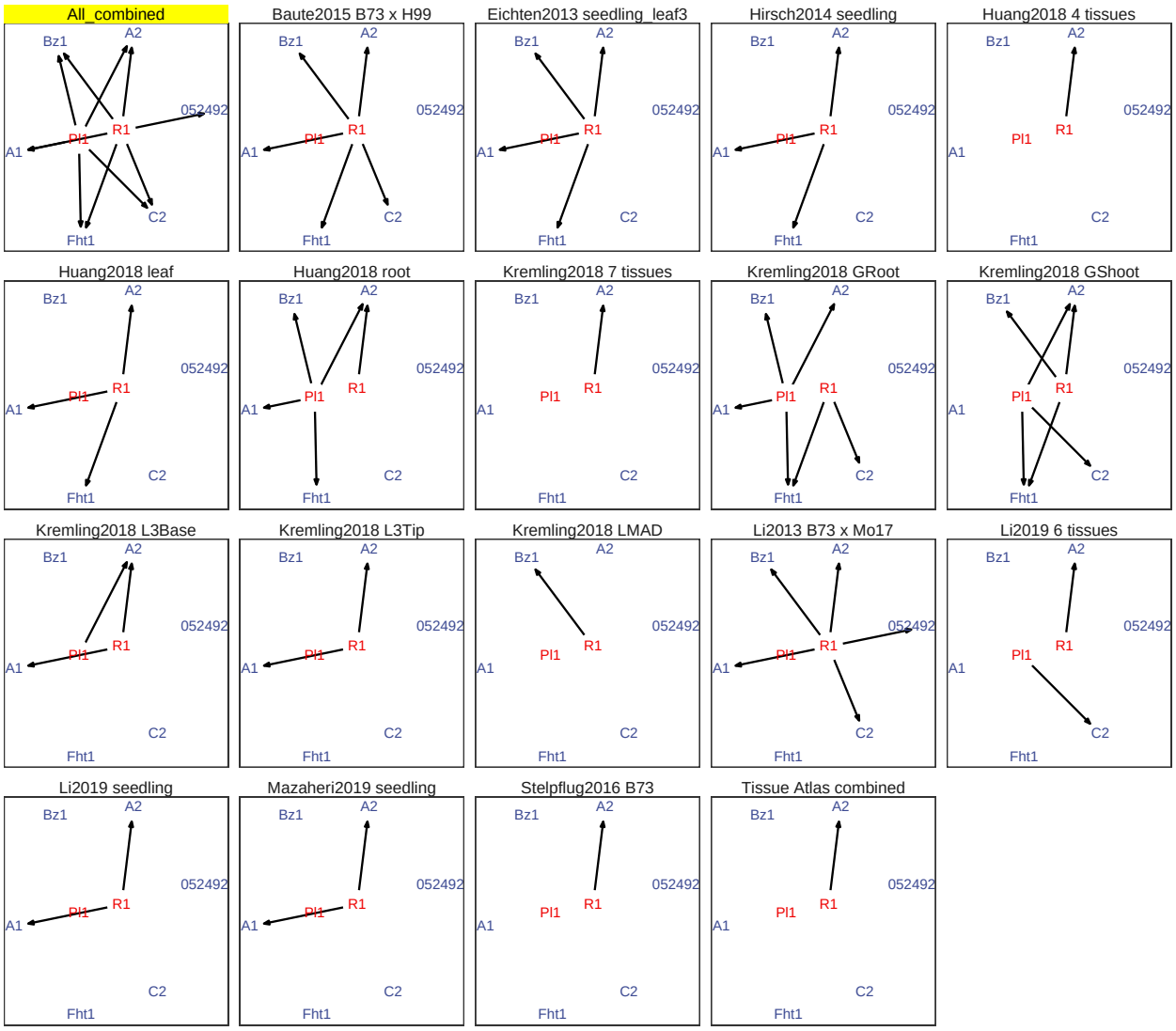

Figure S12. Different GRNs support different parts of the anthocyanin biosynthesis pathway. This supporting figure provides the details to support Figure 4.

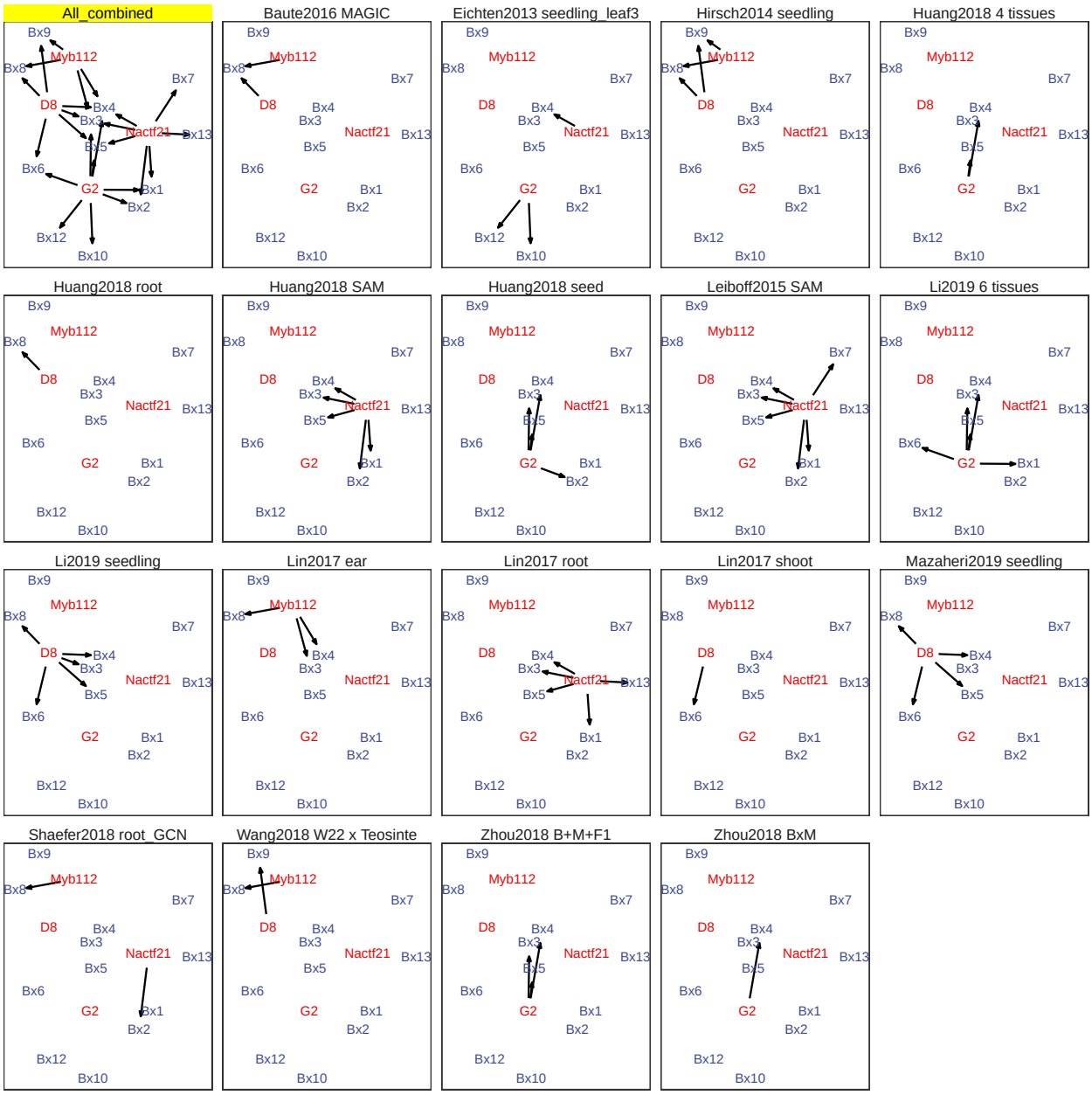

Figure S13. Different GRNs support different parts of the DIMBOA pathway. This supporting figure provides the details to support Figure 4.

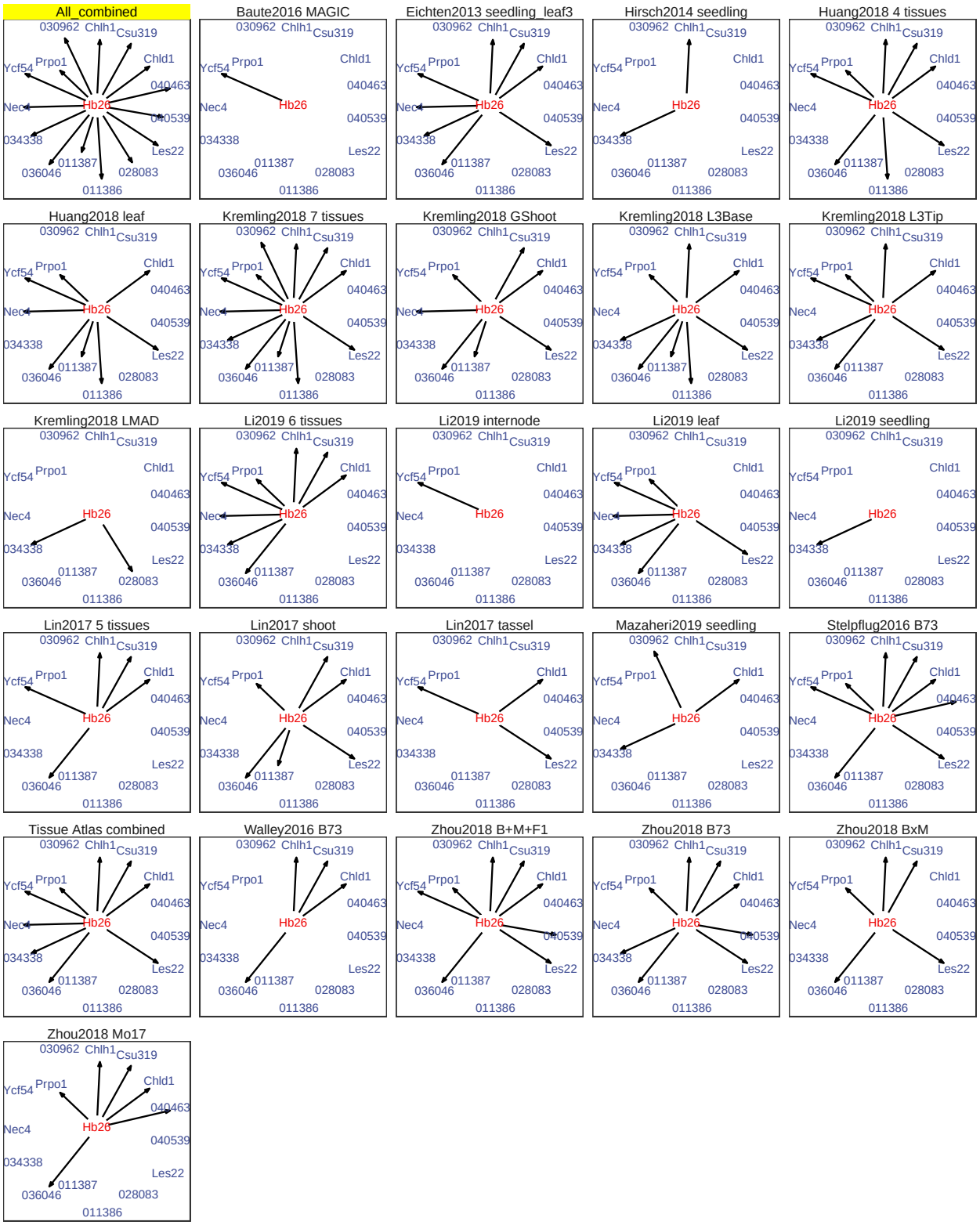

Figure S14. Different GRNs support different parts of the chlorophyllide biosynthesis pathway regulated by a homeobox-transcription factor 26 (HB26, Zm00001d008612). This supporting figure provides the details to support Figure 4.

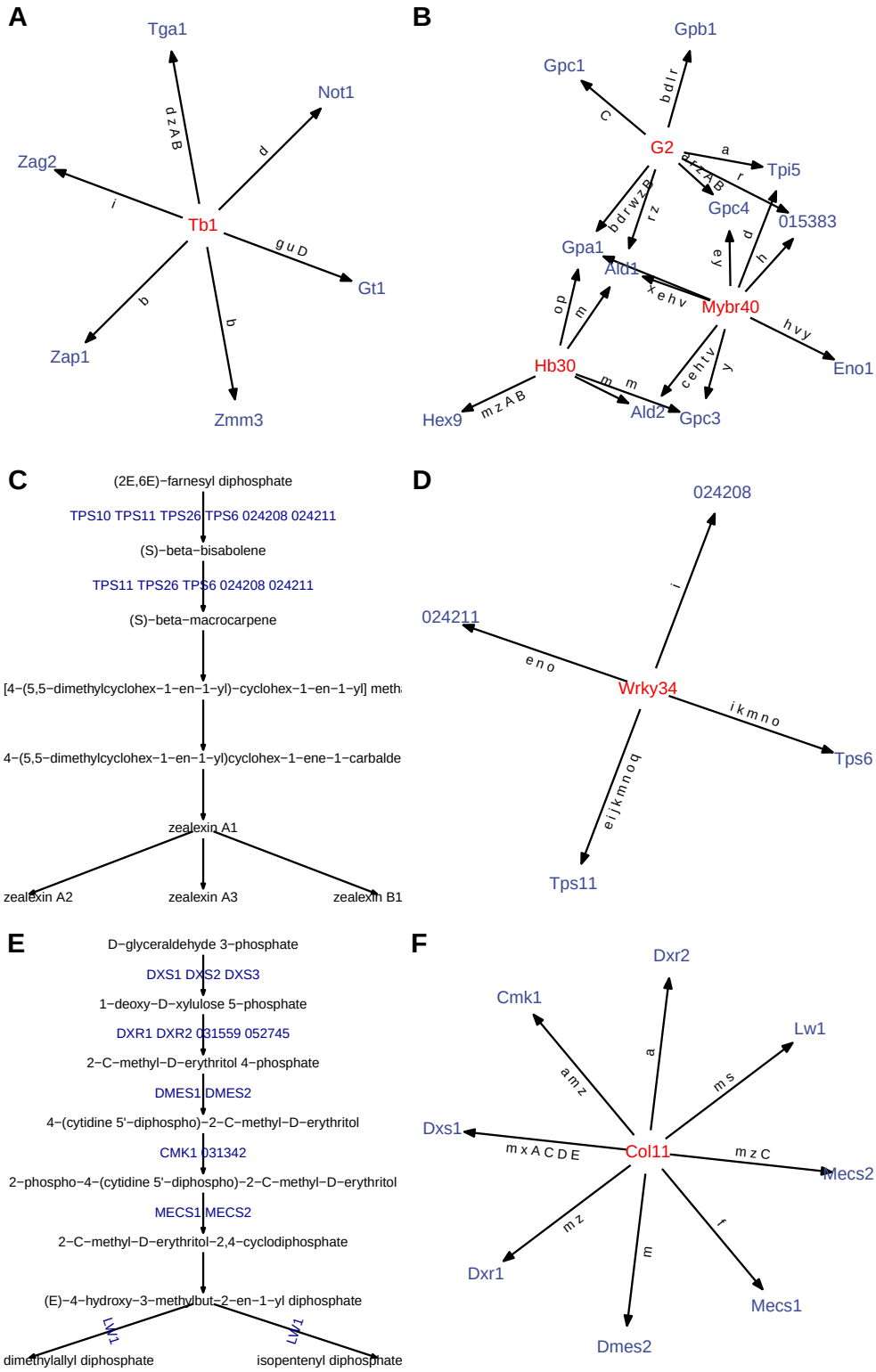

key	network
a	Stelpflug2016 B73
b	Walley2016 B73
c	Yi2019 seed dev
d	Tissue Atlas combined
e	Fu2013 kernel
f	Hirsch2014 seedling
g	Leiboff2015 SAM
h	Shaefer2018 root_GCN
i	Lin2017 5 tissues
j	Lin2017 ear
k	Lin2017 root
l	Lin2017 shoot
m	Kremling2018 7 tissues
n	Kremling2018 GRoot
o	Kremling2018 GShoot
p	Kremling2018 L3Base
q	Kremling2018 LMAN
r	Huang2018 4 tissues
s	Huang2018 leaf
t	Huang2018 root
u	Huang2018 SAM
v	Huang2018 seed
w	Li2019 6 tissues
x	Li2019 internode
y	Li2019 shoot
z	Zhou2018 B+M+F1
A	Zhou2018 B73
B	Zhou2018 Mo17
C	Zhou2018 BxM
D	Li2013 B73 x Mo17
E	Baute2015 B73 x H99

Figure S15. Different coexpression-based GRNs capture distinct parts of classic and CornCyc metabolic pathways. (A) The teosinte branched1 (tb1)-mediated pathway regulating bud dormancy and growth repression. (B) The glycolysis pathway. (C-D) The zealexin biosynthesis pathway (C) regulated by a WRKY-transcription factor 34 (WRKY34, Zm00001d009939) (D). (E-F) The methylerythritol phosphate pathway

(E) regulated by a C2C2-CO-like-transcription factor 11 (COL11, Zm00001d003162) (F). The letters along the edges of the networks in (B) (D) and (F) indicate significant support from specific GRN as indicated in the key. This supporting figure provides the additional examples to support Figure 4.

non_DE DE1−2 DE2−4 DE4+ SPE

Marcon2017 root_control: B73 vs Mo17
Marcon2017 root_drought: B73 vs Mo17
Sun2018 bract: B73 vs Mo17
Sun2018 endosperm: B73 vs Mo17
Sun2018 root: B73 vs Mo17
Sun2018 seedling: B73 vs Mo17
Sun2018 stem: B73 vs Mo17
Waters2017 leaf3_cold: B73 vs B37
Waters2017 leaf3_cold: B73 vs Mo17
Waters2017 leaf3_cold: B73 vs Oh43
Waters2017 leaf3_cold: B73 vs PH207
Waters2017 leaf3_control: B73 vs B37
Waters2017 leaf3_control: B73 vs Mo17
Waters2017 leaf3_control: B73 vs Oh43
Waters2017 leaf3_control: B73 vs PH207
Waters2017 leaf3_heat: B73 vs B37
Waters2017 leaf3_heat: B73 vs Mo17
Waters2017 leaf3_heat: B73 vs Oh43
Waters2017 leaf3_heat: B73 vs PH207
Zhou2018 auricle: B73 vs Mo17
Zhou2018 blade_leaf: B73 vs Mo17
Zhou2018 coleoptile: B73 vs Mo17
Zhou2018 ear: B73 vs Mo17
Zhou2018 embryo: B73 vs Mo17
Zhou2018 endosperm14D: B73 vs Mo17
Zhou2018 endosperm27D: B73 vs Mo17
Zhou2018 flag_leaf: B73 vs Mo17
Zhou2018 floret: B73 vs Mo17
Zhou2018 husk: B73 vs Mo17
Zhou2018 internode: B73 vs Mo17
Zhou2018 kernel: B73 vs Mo17
Zhou2018 radicle_root: B73 vs Mo17
Zhou2018 root: B73 vs Mo17
Zhou2018 seed_imbibed: B73 vs Mo17
Zhou2018 seedling_leaf: B73 vs Mo17
Zhou2018 seedling_meristem: B73 vs Mo17
Zhou2018 seedling_root: B73 vs Mo17
Zhou2018 sheath: B73 vs Mo17
Zhou2018 silk: B73 vs Mo17
Zhou2018 spikelet: B73 vs Mo17
Zhou2018 tassel_stem: B73 vs Mo17
Zhou2018 tassel: B73 vs Mo17

Proportion targets that are DE

Edge score

Figure S16. TF-target validation of the combined tissue network in all six selected natural variation datasets. Each panel shows the proportion of differentially expressed targets regulated by TFs showing different DE levels between two genotypes in one tissue/treatment condition. TF-target predictions were binned to 10 groups based on the interaction score in GRN. Each TF-target pair is classified according to the DE level of the TF ("non_DE", "DE1-2", "DE2-4", "DE4+" or "SPE") in each network. The proportion of TF-target pairs with the target also showing DE was then determined for each category. Within each panel the actual numbers of TF-target pairs falling into the "SPE" category (i.e., purple line) were labelled next to each point. Dashed line in each panel represents the genome-wide (background) proportion of DE genes in each tissue/treatment setting. This provides the full set of panels to support the interpretations of Figure 5.

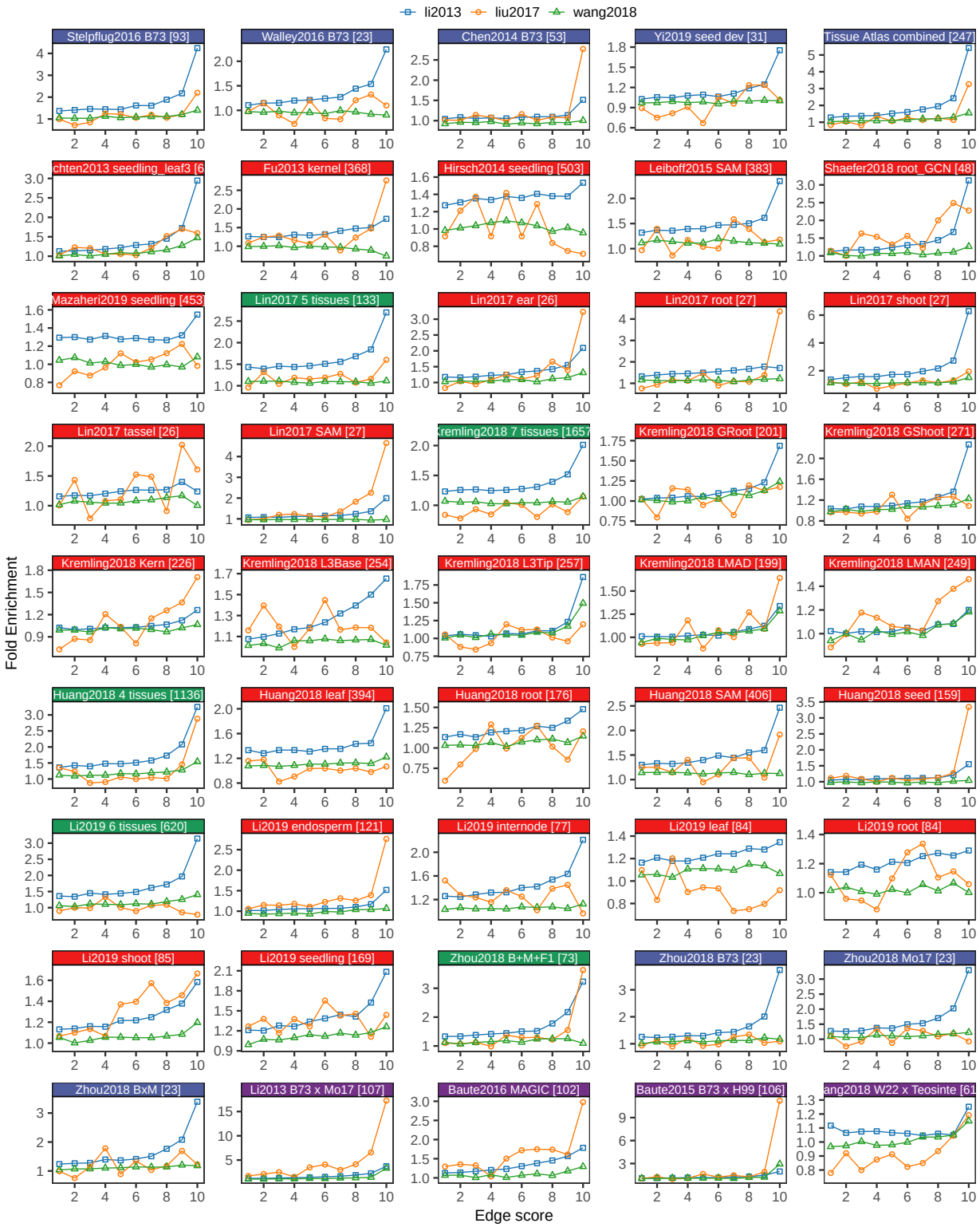

Figure S17. Enrichment of co-regulated targets between previously identified trans-eQTL hotspots and TF-target associations predicted by GRNs. For each network the top 1 million TF-target predictions were binned to 10 groups based on the interaction score in GRN. Fold enrichment is determined by the same permutation approach described in Figure 2. The analyses here support the interpretations of Figure 7.

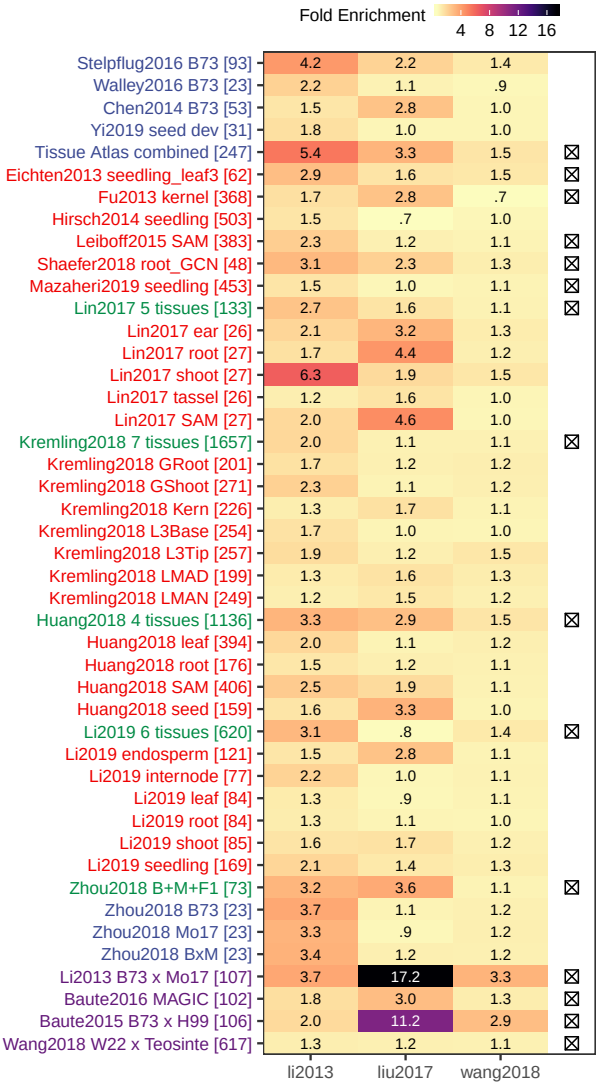

Figure S18. Enrichment of co-regulated targets between previously identified trans-eQTL hotspots and TF-target associations predicted by GRNs. For each network the top 1 million predicted TF-target associations were binned to 10 bins and only the first bin (top 100k edges) were used to assess enrichment. 15 high quality networks (marked with crosses) were selected to identify the main TF regulators underlying trans-eQTL hotspots (see Methods). The analyses here support the interpretations of Figure 7.

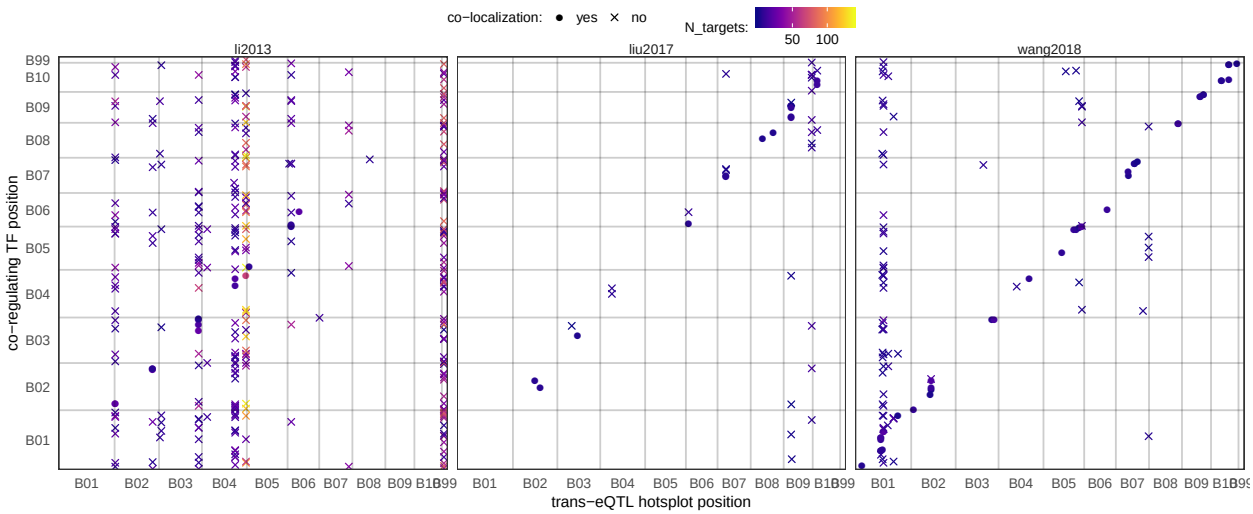

Figure S19. Co-localization of TFs predicted by GRNs in this study and trans-eQTL hotspots identified in previous studies that regulate the same set of targets. Each trans-eQTL hotspot were first tested for significant overlap in targets with any TFs (hypergeometric enrichment test as implemented in the phyper() function in R). To control for false positives, only TFs identified in at least two (out of 8 high quality networks, see Methods) that show significant co-regulation with at least one trans-eQTL hotspot ($p < 0.01$) were kept. Trans-eQTL hotspots identified in previous maize assemblies were lifted over to the AGPv4 assembly coordinates. Co-localization of a TF and a trans-eQTL is determined if the two coordinates are within 50-Mbp distance. Color of each dot represents the number of common targets between the predicted TF regulator and the trans-eQTL hotspot. The analyses here support the interpretations of Figure 7.

Table S1. ChIP-Seq and DAP-Seq datasets used in this study.

TF alias	TF name	TF ID	Tissue	Study Type	Targets	Reference
KN1	knotted1	Zm00001d033859	ear, leaf, tassel, SAM	ChIP-seq	648	Bolduc2012
P1	pericarp color1	Zm00001d028854	endosperm	ChIP-seq	20	Morohashi2012
RA1	ramosa1	Zm00001d020430	ear	ChIP-seq	203	Eveland2014
FEA4	fascinated ear4	Zm00001d037317	ear	ChIP-seq	99	Pautler2015
HDA101	histone deacetylase homolog	Zm00001d053595	seed	ChIP-seq	112	Yang2016
O2	opaque2	Zm00001d018971	endosperm	ChIP-seq	32	Zhan2018
bZIP22	bZIP-transcription factor 22	Zm00001d021191	kernel	ChIP-seq	25	Li2018
TB1	teosinte brach1	Zm00001d033673	tiller bud	ChIP-seq	3445	Dong2019
ARF10		Zm00001d042267		DAP-seq		Galli2018
ARF13		Zm00001d049295		DAP-seq		Galli2018
ARF14		Zm00001d050781		DAP-seq		Galli2018
ARF16		Zm00001d053819		DAP-seq		Galli2018
ARF18		Zm00001d014377		DAP-seq		Galli2018
ARF25		Zm00001d011953		DAP-seq		Galli2018
ARF27		Zm00001d045026		DAP-seq		Galli2018
ARF29		Zm00001d026540		DAP-seq		Galli2018
ARF34		Zm00001d031064		DAP-seq		Galli2018
ARF35		Zm00001d014690		DAP-seq		Galli2018
ARF36		Zm00001d016838		DAP-seq		Galli2018
ARF39		Zm00001d003601		DAP-seq		Galli2018
ARF4		Zm00001d001945		DAP-seq		Galli2018
ARF7		Zm00001d039267		DAP-seq		Galli2018
BAD1		Zm00001d005737		DAP-seq		Ricci2019
BZIP25		Zm00001d010658		DAP-seq		Ricci2019
BZIP54		Zm00001d022542		DAP-seq		Ricci2019
BZIP57	FEA4	Zm00001d037317		DAP-seq		Ricci2019
BZIP72		Zm00001d008225		DAP-seq		Ricci2019
BZIP96		Zm00001d010638		DAP-seq		Ricci2019
EREB127		Zm00001d051451		DAP-seq		Ricci2019
EREB138		Zm00001d015639		DAP-seq		Ricci2019
EREB24	BBM	Zm00001d002025		DAP-seq		Ricci2019
EREB29		Zm00001d012584		DAP-seq		Ricci2019
EREB71		Zm00001d048208		DAP-seq		Ricci2019
LBD16	RA2	Zm00001d039694		DAP-seq		Ricci2019
LBD19	IG1	Zm00001d042560		DAP-seq		Ricci2019
LBD38		Zm00001d010751		DAP-seq		Ricci2019
LBD5		Zm00001d029506		DAP-seq		Ricci2019
SBP30	UB3	Zm00001d052890		DAP-seq		Ricci2019
SBP6		Zm00001d012916		DAP-seq		Ricci2019
SBP8	UB2	Zm00001d031451		DAP-seq		Ricci2019

Table S2. TF knockout mutant RNA-Seq datasets used in this study.

TF alias	TF name	TF ID	Tissue	Reference
KN1	knotted1	Zm00001d033859	ear, leaf, tassel, SAM	Bolduc2012
P1	pericarp color1	Zm00001d028854	endosperm	Morohashi2012
RA1	ramosa1	Zm00001d020430	ear	Eveland2014
RA2	ramosa2	Zm00001d039694	ear	Eveland2014
RA3	ramosa3	Zm00001d022193	ear	Eveland2014
FEA4	fascinated ear4	Zm00001d037317	ear	Pautler2015
HDA101	histone deacetylase homolog	Zm00001d053595	seed	Yang2016
NKD1	naked endosperm1	Zm00001d002654	aleurone, endosperm	Gontarek2016
O2	opaque2	Zm00001d018971	endosperm	Zhan2018
bZIP22	bZIP-transcription factor 22	Zm00001d021191	kernel	Li2018
TB1	teosinte brach1	Zm00001d033673	tiller bud	Dong2019
GT1	grassy tillers1	Zm00001d028129	tiller bud	Dong2019

Table S3. Natural variation datasets used for validation in this study.

author	study	condition	contrast	non-DE	DE1-2	DE2-4	DE4+	SPE
Waters2017	stress cis-trans	leaf3 cold	B73 vs B37	14,991	5,508	2,524	2,191	765
		leaf3 cold	B73 vs Oh43	13,985	6,013	2,955	2,226	800
		leaf3 control	B73 vs B37	11,868	7,131	3,468	2,551	961
		leaf3 control	B73 vs Oh43	12,804	6,395	3,213	2,545	1,022
		leaf3 heat	B73 vs B37	14,488	5,491	2,937	2,276	787
		leaf3 heat	B73 vs Oh43	13,304	5,931	3,249	2,568	927
		leaf3 cold	B73 vs Mo17	17,235	2,783	2,136	1,550	796
		leaf3 cold	B73 vs PH207	17,202	3,023	2,075	1,439	761
		leaf3 control	B73 vs Mo17	18,843	2,012	1,610	1,226	809
		leaf3 control	B73 vs PH207	19,148	1,868	1,447	1,239	798
		leaf3 heat	B73 vs Mo17	18,453	2,433	1,641	1,152	821
		leaf3 heat	B73 vs PH207	16,533	3,404	2,312	1,459	792
Marcon2017	drought stress	root control	B73 vs Mo17	13,185	6,718	2,513	1,940	651
		root drought	B73 vs Mo17	13,828	6,370	2,347	1,864	598
Sun2018	mo17 genome	bract	B73 vs Mo17	19,008	832	980	1,192	702
		endosperm	B73 vs Mo17	18,841	1,021	1,240	1,016	596
		root	B73 vs Mo17	18,760	820	1,114	1,371	649
		seedling	B73 vs Mo17	19,416	661	850	980	807
		stem	B73 vs Mo17	18,669	887	1,130	1,164	864
Zhou2018	B73 Mo17 atlas	auricle	B73 vs Mo17	14,944	3,885	2,596	2,091	860
		blade leaf	B73 vs Mo17	16,331	3,174	2,170	1,775	926
		coleoptile	B73 vs Mo17	18,653	2,392	1,389	1,367	575
		ear	B73 vs Mo17	18,838	2,425	1,213	1,095	805
		embryo	B73 vs Mo17	16,351	3,577	2,227	1,407	814
		endosperm14D	B73 vs Mo17	17,848	2,570	1,748	1,468	742
		endosperm27D	B73 vs Mo17	16,695	3,105	2,254	1,458	864
		flag leaf	B73 vs Mo17	16,090	3,146	2,329	1,898	913
		floret	B73 vs Mo17	17,037	3,259	1,977	1,342	761
		husk	B73 vs Mo17	16,723	3,362	1,809	1,605	877
		internode	B73 vs Mo17	13,644	4,273	2,844	2,653	962
		kernel	B73 vs Mo17	17,590	2,946	1,734	1,362	744
		radicle root	B73 vs Mo17	18,120	2,346	1,764	1,501	645
		root	B73 vs Mo17	17,334	2,883	1,844	1,499	816
		seed imbibed	B73 vs Mo17	12,068	5,342	3,606	2,626	734
		seedling leaf	B73 vs Mo17	16,245	2,938	2,286	2,079	828
		seedling meristem	B73 vs Mo17	19,207	1,923	1,249	1,235	762
		seedling root	B73 vs Mo17	18,842	2,009	1,631	1,180	714
		sheath	B73 vs Mo17	15,209	3,885	2,633	1,810	839
		silk	B73 vs Mo17	15,378	3,577	2,303	2,152	966
		spikelet	B73 vs Mo17	17,984	2,736	1,589	1,209	858
		tassel	B73 vs Mo17	15,594	3,856	2,435	1,677	814
		tassel stem	B73 vs Mo17	12,564	4,625	3,512	2,652	1,023

Table S4. GRN-predicted TFs supported by trans-eQTL hotspots.

ID	Support eQTL study	Support GRN	TF Annotation	Target enrichment
Zm00001d001945	li2013, wang2018	fu2013, leiboff2015, lin2017, li2019, wang2018, huang2018, zhou2018, li2013, baute2015	Auxin response factor 4	(25) histone H3-K9 methylation; (9) cytokinesis by cell plate formation; (8) cell proliferation
Zm00001d003162	li2013	tissue atlas, leiboff2015, mazaheri2019, huang2018, li2013, kremling2018, zhou2018, baute2016, baute2015	Zinc finger protein CONSTANS-LIKE 5	(57) cysteine biosynthetic process; (45) photosynthesis, light harvesting in photosystem I; (38) photosynthesis light reactions; (16) rRNA processing; (15) photosystem II assembly; (8) Calvin-Benson-Bassham cycle
Zm00001d003195	li2013	tissue atlas, zhou2018	Salt tolerance-like protein	(9) rRNA processing; (8) Calvin-Benson-Bassham cycle
Zm00001d004095	wang2018	li2013, baute2016	basic helix-loop-helix (bHLH) DNA-binding superfamily protein	
Zm00001d004358	wang2018	baute2016, wang2018		(11) pentose-phosphate shunt
Zm00001d004497	liu2017, wang2018	baute2015, wang2018, baute2016	C2H2-like zinc finger protein	
Zm00001d005016	liu2017, wang2018	baute2016, baute2015	WRI1 transcription factor1	(22) glycolysis I (from glucose 6-phosphate)
Zm00001d006578	li2013	li2013, baute2015	Transcription factor bHLH130	(11) L-alanine degradation II (to D-lactate)
Zm00001d006701	li2013	li2013, baute2015	GRAS transcription factor	(6) C4 photosynthetic carbon assimilation cycle, PEPCK type
Zm00001d006721	li2013	li2013, baute2015	Protein SHORT-ROOT	
Zm00001d010060	liu2017	baute2015, wang2018	BEL1-like homeodomain protein 9	
Zm00001d010785	liu2017	li2013, baute2015	Putative GATA transcription factor family protein	
Zm00001d012544	wang2018	li2013, baute2015	myb domain protein 81	(6) glycolysis I (from glucose 6-phosphate)
Zm00001d012605	wang2018	li2013, baute2015	MRP interacting1	
Zm00001d013547	li2013	li2013, baute2015	BEL1-like homeodomain protein 3	
Zm00001d015412	wang2018	li2013, baute2015	sequence-specific DNA binding transcription factors	(10) suberin monomers biosynthesis
Zm00001d017788	wang2018	li2013, baute2016, baute2015	Dof zinc finger protein DOF2.1	
Zm00001d017900	wang2018	li2013, wang2018	Dof zinc finger protein DOF5.4	
Zm00001d018225	wang2018	li2013, baute2016	Homeodomain leucine zipper family IV protein	(27) triacylglycerol degradation; (15) phenylpropanoid biosynthesis; (11) very long chain fatty acid biosynthesis I
Zm00001d018465	wang2018	li2013, baute2016, baute2015		
Zm00001d020019	liu2017	li2013, baute2016, baute2015	Protein PHR1-LIKE 3	
Zm00001d020043	liu2017, wang2018	li2013, baute2016, baute2015	Ethylene-responsive transcription factor ERF117	

Zm00001d020408	wang2018	li2013, baute2015	Typical P-type R2R3 Myb protein	
Zm00001d021403	wang2018	li2013, baute2015	indeterminate1 domain7	(9) UDP-sugars interconversion
Zm00001d021442	wang2018	mazaheri2019, baute2015	Protein NLP2	(6) sucrose degradation II (sucrose synthase)
Zm00001d021701	wang2018	li2013, wang2018	Transcription factor ILR3	
Zm00001d024041	liu2017	li2013, baute2015	bZIP transcription factor 16	
Zm00001d024230	liu2017, wang2018	li2013, baute2015	Nuclear transcription factor Y subunit C-2	
Zm00001d024268	wang2018	li2013, baute2015	NAC domain-containing protein 21/22	
Zm00001d024323	wang2018	eichten2013, baute2015	Putative WRKY DNA-binding domain superfamily protein	(48) flavonoid biosynthesis (in equisetum); (16) anthocyanin biosynthesis
Zm00001d026147	wang2018	eichten2013, li2013, baute2015	plant color component at R1	(14) L-glutamine degradation I; (12) anthocyanin biosynthesis; (11) glycerophosphodiester degradation; (10) flavonoid biosynthesis (in equisetum)
Zm00001d026271	wang2018	li2013, baute2015	Putative AP2/EREBP transcription factor superfamily protein	
Zm00001d026448	wang2018	li2013, baute2015	Floral homeotic protein APETALA 2	(11) proanthocyanidins biosynthesis from flavanols
Zm00001d028007	wang2018	baute2016, baute2015	Calmodulin-binding transcription activator 2	(26) gluconeogenesis I; (7) fatty acid biosynthesis initiation I
Zm00001d029934	wang2018	li2013, baute2015	Homeobox-leucine zipper protein HAT4	
Zm00001d029963	wang2018	baute2015, wang2018	myb-like transcription factor family protein	
Zm00001d030028	li2013, wang2018	leiboff2015, huang2018, li2013, baute2016, baute2015	myc transcription factor7	(48) response to wounding; (15) cutin biosynthesis; (10) regulation of transcription, DNA-templated; (8) jasmonic acid biosynthesis; (6) regulation of transcription, DNA-templated; (5) response to wounding
Zm00001d030727	wang2018	li2013, baute2015	Dof zinc finger protein DOF2.2	(11) cell proliferation; (9) regulation of transcription, DNA-templated
Zm00001d030907	wang2018	li2013, baute2015	B3 domain-containing protein	
Zm00001d030908	wang2018	li2013, baute2015	B3 domain-containing protein	
Zm00001d031561	wang2018	baute2015, wang2018	Transcription factor bHLH62	(24) response to wounding; (7) response to wounding
Zm00001d031665	wang2018	baute2016, baute2015	Transcription factor bHLH137	(12) triacylglycerol degradation
Zm00001d033898	li2013, wang2018	tissue atlas, lin2017, li2019, zhou2018, kremling2018, huang2018, baute2016, baute2015	BEL1-like homeodomain protein 4	(34) Calvin-Benson-Bassham cycle; (23) photosystem II assembly; (10) rRNA processing; (9) isopentenyl diphosphate biosynthetic process, methylerythritol 4-phosphate pathway; (7) gluconeogenesis I; (7) photosynthesis light reactions; (7) response to cytokinin; (7) positive regulation of transcription, DNA-templated; (6) photosynthetic electron transport in photosystem I; (5) response to salt stress

Zm00001d034984	li2013	tissue atlas, zhou2018	Putative NAC domain transcription factor superfamily protein	
Zm00001d035084	li2013	shaefer2018, baute2015, li2013, baute2016	Putative NAC domain transcription factor superfamily protein	
Zm00001d035195	li2013	tissue atlas, huang2018	Protein LSD1	(6) GDP-mannose biosynthesis
Zm00001d035224	liu2017	lin2017, zhou2018	protein	
Zm00001d036214	li2013	li2013, baute2016	B-box zinc finger protein 22	(20) glycolysis I (from glucose 6-phosphate)
Zm00001d036364	wang2018	eichten2013, kremling2018, wang2018	NAC domain containing protein 36	(8) glycerophosphodiester degradation
Zm00001d041831	liu2017	baute2016, baute2015	DNA binding protein	
Zm00001d042463	li2013	huang2018, li2013	Two-component response regulator ARR11	
Zm00001d043420	li2013	kremling2018, baute2016, shaefer2018, li2019, tissue atlas, lin2017, zhou2018, li2013	Basic leucine zipper 34	(20) homogalacturonan degradation
Zm00001d044260	li2013, wang2018	li2013, baute2015	C3H-type transcription factor	
Zm00001d044355	wang2018	li2013, baute2015	B3 domain-containing protein	
Zm00001d044538	li2013	huang2018, zhou2018		(8) regulation of transcription by RNA polymerase II; (7) cellulose biosynthesis; (7) triacylglycerol degradation
Zm00001d045581	liu2017	li2013, baute2016, baute2015	Putative MYB DNA-binding domain superfamily protein	
Zm00001d045661	li2013, liu2017, wang2018	tissue atlas, eichten2013, mazaheri2019, lin2017, kremling2018, huang2018, li2019, zhou2018, li2013, baute2015	Zinc finger protein CONSTANS-LIKE 16	(66) rRNA processing; (21) photosynthesis light reactions; (14) photosynthesis, light harvesting in photosystem I; (12) thylakoid membrane organization; (12) RNA modification; (10) response to cytokinin; (7) Calvin-Benson-Bassham cycle; (6) chloroplast organization
Zm00001d046323	liu2017	fu2013, li2013, baute2016, baute2015		
Zm00001d046405	li2013, liu2017, wang2018	tissue atlas, eichten2013, lin2017, kremling2018, huang2018, li2019, zhou2018, baute2016, wang2018, leiboff2015, shaefer2018, li2013, baute2015	Putative homeodomain-like transcription factor superfamily protein	(89) isopentenyl diphosphate biosynthetic process, methylerythritol 4-phosphate pathway; (60) thylakoid membrane organization; (24) 3,8-divinyl-chlorophyllide a biosynthesis I (aerobic, light-dependent); (18) positive regulation of transcription, DNA-templated; (13) pyrimidine ribonucleotides interconversion; (12) RNA modification; (10) chloroplast organization; (10) palmitate biosynthesis II (bacteria and plants); (6) chloroplast organization; (6) tetrapyrrole biosynthesis I (from glutamate)
Zm00001d046441	liu2017	li2013, baute2016, baute2015	FAR1-domain family sequence	(7) formate oxidation to CO₂

Zm00001d047519	li2013, wang2018	leiboff2015, shaefer2018, lin2017, li2013, baute2015	basic leucine-zipper 52	(15) cell proliferation
Zm00001d047563	wang2018	li2013, baute2015	ethylene insensitive-like1	(6) translation
Zm00001d047968	wang2018	li2013, baute2015	Zinc finger protein 1	
Zm00001d047999	wang2018	li2013, baute2015	Putative HLH DNA-binding domain superfamily protein	
Zm00001d051573	li2013	leiboff2015, lin2017, zhou2018	Putative homeobox DNA-binding domain superfamily protein	
Zm00001d052798	li2013	leiboff2015, shaefer2018, li2013	Homeodomain-like superfamily protein	
Zm00001d052847	wang2018	li2013, baute2016, baute2015	Putative WRKY DNA-binding domain superfamily protein	
Zm00001d053124	li2013	tissue atlas, kremling2018, huang2018, li2019, zhou2018	myb domain protein 60	(33) thylakoid membrane organization; (30) isopentenyl diphosphate biosynthetic process, methylerythritol 4-phosphate pathway; (22) rRNA processing; (17) triacylglycerol degradation; (11) response to cold; (9) chloroplast organization; (7) photosystem II assembly; (7) Calvin-Benson-Bassham cycle; (5) photosynthesis light reactions; (5) RNA modification